Brain Pathology ISSN 1015-6305

RESEARCH ARTICLE

Oligodendrocyte Lineage Cells in Chronic Demyelination of Multiple Sclerosis Optic Nerve

Alison Ruth Jennings[1]; William M. Carroll[1,2]

[1] School of Pathology and Laboratory Medicine, University of Western Australia, Nedlands, WA, Australia.
[2] Department of Neurology, Sir Charles Gairdner Hospital, Nedlands, WA, Australia.

Keywords
chronic demyelination, multiple sclerosis, oligodendrocytes, optic nerve, remyelination failure.

Corresponding author:
Alison Ruth Jennings, PhD, School of Pathology and Laboratory Medicine, University of Western Australia, M Block, QEII Medical Centre, Hospital Ave., Nedlands, WA 6009, Australia
(E-mail: *alison.jennings@uwa.edu.au*)

Received 24 July 2014
Accepted 26 August 2014
Published Online Article Accepted 29 August 2014

doi:10.1111/bpa.12193

Abstract

Reports that chronically demyelinated multiple sclerosis brain and spinal cord lesions contained immature oligodendrocyte lineage cells have generated major interest aimed at the potential for promotion of endogenous repair. Despite the prominence of the optic nerve as a lesion site and its importance in clinical disease assessment, no detailed studies of multiple sclerosis-affected optic nerve exist. This study aims to provide insight into the cellular pathology of chronic demyelination in multiple sclerosis through direct morphological and immunohistochemical analysis of optic nerve in conjunction with observations from an experimental cat optic nerve model of successful remyelination. Myelin staining was followed by immunohistochemistry to differentially label neuroglia. Digitally immortalized sections were then analyzed to generate quantification data and antigenic phenotypes including maturational stages within the oligodendrocyte lineage. It was found that some chronically demyelinated multiple sclerosis optic nerve lesions contained oligodendroglial cells and that heterogeneity existed in the presence of myelin sheaths, oligodendrocyte maturational stages and extent of axonal investment. The findings advance our understanding of oligodendrocyte activity in chronically demyelinated human optic nerve and may have implications for studies aimed at enhancement of endogenous repair in multiple sclerosis.

INTRODUCTION

A hallmark of multiple sclerosis (MS) is the eventual predominance of chronically demyelinated "sclerotic" plaques despite evidence of successful remyelination, particularly in the early phases of the disease. Recently, it has been reported that some chronic demyelination lesions in the brain and spinal cord contained immature phenotype oligodendrocyte lineage cells (14, 34, 39, 58, 59, 61). Based on these reports, a tenet has emerged that remyelination failure despite the presence of immature oligodendrocytes is a widespread feature of chronic demyelination lesions in MS (32–34). Stimulated by the prospect of therapeutic intervention to promote functional repair, numerous experimental studies have since generated hypotheses to explain why remyelination fails in MS (22, 41, 50, 62, 64).

However, given the relatively few instances of direct investigation of chronic MS lesions on which the concept of remyelination failure has been based and also the inter-study variation in observed pathology, there is a need for further examples to be described with particular emphasis on the presence and maturational stages of the resident oligodendroglial cells and whether lesions are quiescent (34, 59, 61) or display active cell turnover (14, 39).

The optic nerve (ON) provides an ideal setting for investigation of endogenous repair in MS lesions with regular, aligned fiber bundles and a relatively simple, well-characterized neuroglial complement, conducive to both qualitative and quantitative analyses (28). It is also a major lesion site in MS (1, 2, 13, 19, 51). However, despite extensive statistics on the incidence of optic neuritis and the obvious relevance to MS, few studies have specifically investigated the microscopic pathology of multiple sclerosis optic nerve (MSON) lesions (20) and, to the best of our knowledge, none have employed immunohistochemistry (IHC).

The present study describes the pathology found in archival samples of chronically demyelinated MSON. Characterization of the neuroglia was aided by previous studies of normal cat and human ON (28). Similarly, the stage-specific identification of oligodendroglial cells within demyelinated lesions was made possible by reference to the experimental cat optic nerve (ECON) model of demyelination and remyelination in which individual cell antigenic phenotypes have been correlated with ultrastructural detail, including relationship to demyelinated axons (7, 27). We report the presence of oligodendroglial cells in some chronically demyelinated MSON lesions. Although all such lesions were stable and quiescent, significant inter- and intra-lesion heterogeneity existed in oligodendrocyte maturational stages and the extent of their axonal investment.

Table 1. Stains; primary antibodies; secondary antibodies; chromogens.
Abbreviations: AP = alkaline phosphatase; G = goat; Ig = immunoglobulin; m = mouse/monoclonal; OI = oligodendrocyte; OP = oligodendrocyte progenitor cell; OPC = oligodendrocyte precursor cell; p = polyclonal; premyOI = premyelinating OI; remyOI = remyelinating OI; rb = rabbit.

Marker abbrev	Name/detail	Dilution	Target	Source
LFB	Luxol fast blue		Myelin	Sigma
SoC	Solochrome (eriochrome) cyanine		Myelin	Sigma
NF	Pan neurofilament; p IgG	1:5000	Axonal neurofilaments	Affiniti
Ki-67	Ki-67 m IgM clone PP-67	1:800	Nuclear antigen in proliferating cells	Sigma
GFAP	Glial fibrillary acidic protein; p	1:2000	Astrocytes	Dako
Vim	Vimentin; m anti-swine clone V9 rb mono clone SP20	1:200 1:400	Astrocytes, microglia (activated), oligodendroglia (OPC)	Dako; Spring
CAII	Carbonic anhydrase isoenz II; m	1:400	Oligodendroglia (OI)	Santa Cruz
MBP	Myelin basic protein; m	1:300	Myelin; oligodendroglia (remyOI)	NCL
HNK-1	Human natural killer cell/CD57; m IgM—biotin	1:50	Oligodendroglia (premyOI; remyOI; OI)	BD
GS	Glutamine synthetase	1:800	Oligodendroglia (premyOI; remyOI; OI)	BD
NoA	Nogo-A; p IgG	1:4000	Oligodendroglia (premyOI; remyOI; OI)	Santa Cruz
PLP	Proteolipid protein AA3 including isoform DM20; rat m	1:400	Myelin; oligodendroglia (premyOI; remyOI)	W. Macklin
p25	P25a/TPPP (tubulin polymerization promoting protein); m	1:2000	Oligodendroglia (remyOI; OI)	J. Ovadi
Olig1	OI transcription factor 1; p	1:400 1:2000	Oligodendroglial lineage (nuclear in OP; OPC)	RnD; C. Stiles
Olig2	OI transcription factor 2; p	1:12000	Oligodendroglial lineage (nuclear)	C. Stiles
GSLII	Griffonia simplicifolia isolectin II	1:20	Oligodendroglia (remyOI; OI); microglia (activated)/macrophage	Vector
Fcg/γ	HPA010718; p IgG	1:600	Microglia/macrophage	Sigma
CD68	CD68; m IgG1k clone KP1	1:400	Microglia/macrophage	Dako
RCA-1	Ricinus communis agglutinin I	1:1500	Microglia/macrophage	Vector
EV	EnVision		G anti-rb/g anti-m Fab fragment linked to peroxidase-labeled dextran polymer	Dako
NL	NovoLink polymer		Anti-m/rb IgG –p HRP	NCL
mAP	Monoclonal alkaline phosphatase link		G anti-m IgG conjugated to AP	Sigma
pAP	Monoclonal alkaline phosphatase link		G anti-rb IgG conjugated to AP	Sigma
AEC	3-Amino-9-ethylcarbazole		Chromogen	Dako
DAB	Diaminobenzidine ImmPACT		Chromogen	Vector
Fuchsin	Fuchsin		Chromogen	Dako

Source addresses: Affiniti Research, Devon, UK; BD Biosciences, San Diego, CA, USA; Dako Corporation, NSW, Australia; Dr Wendy Macklin, University of Colorado Medical School, Denver, CO, USA; Santa Cruz Biotechnology, Santa Cruz, CA, USA; NCL: Leica Novocastra, Newcastle-on-Tyne, UK; Prof Judit Ovadi, Hungarian Academy of Sciences, Budapest, Hungary; Sigma, St Louis, MO, USA; Spring Bioscience, Pleasanton, CA, USA; Vector, Burlingame, CA, USA; RnD: R & D Systems, Abingdon, UK; Prof. C Stiles, Dana-Farber Cancer Institute, Boston, MA, USA.

MATERIALS AND METHODS

Human control optic nerve

Control neuroglial cell quantification and antigenic phenotype data were generated during previous studies of normal human optic nerve (NHON) post-fixed for up to 2 weeks in 10% buffered formalin for relevance to archival MS specimen analysis (28).

MSON

Eight composite tissue blocks (formalin-fixed paraffin-embedded) comprising 22 noncontiguous ON segments from four cases of chronic MS (Table 1) were obtained from Dr. M Esiri (Oxfordshire Clinical Research Ethics Committee Approval No. C02.340).

Demyelinated cat optic nerve

In studies reported previously, demyelinated lesions were created in the intra-orbital ON of young adult cats (9) to follow the process of remyelination (7, 29). For the current study (Table 1), blocks were selected for further analysis that contained focal lesions timed between 9 and 24 days post lesion to coincide with the transition of oligodendrocyte precursor cells to remyelinating oligodendrocytes (7, 8).

Section preparation

Paraffin-embedded human ON tissue blocks, each containing between one and four segments, were sectioned serially at 3 μm. Resin-embedded cat ON segments were sectioned serially in sets comprising 1 μm sections preceding and following "thin" (80 nm)

sections collected on formvar-coated slot aperture grids for electron microscopy. Prior to immunostaining, paraffin sections were dewaxed and hydrated; resin sections were deplasticised and etched (29).

Myelin staining

To distinguish areas of demyelination in human ON, sections were stained with luxol fast blue (LFB) and counterstained with hematoxylin and eosin. Additionally, solochrome cyanine staining was used to label intact sheaths but not degenerate myelin (41). Cat ON resin sections were stained with toluidine blue to highlight the osmium tetroxide taken up by myelin sheaths during processing for electron microscopy.

IHC

For antigen retrieval, slides were microwaved in 0.05% citraconic anhydride (pH 7.4) for 20 minutes at 95°C. Nonspecific protein binding was blocked with 10% normal horse serum in phosphate buffered saline (PBS) and endogenous peroxidase activity blocked with 0.3% hydrogen peroxide for 5 minutes. Sections were incubated overnight with primary antibodies (Table 1) diluted in PBS and binding was revealed with peroxidase- or alkaline phosphatase-substrate chromogens via species- or immunoglobulin subtype-specific secondary link antibodies (Table 1). For dual staining, primary antibodies applied as a cocktail were separately revealed with 3,3′-diaminobenzidine (DAB; brown) vs. 3-amino-9-ethylcarbazole (AEC) or Fuchsin (red) and counterstained with hematoxylin. To maximize staining information from individual paraffin sections, the SIMPLE (Sequential Immunoperoxidase Labeling and Erasing) protocol (24) was modified to incorporate myelin staining as part of the pre- and/or counterstaining regime. Rounds of single primary immunostaining, revealed with the alcohol-soluble chromogen, AEC, were immortalized by digital slide scanning (see below) before chromogen removal and application of the next antibody of interest. Cat lesion serial sections were reacted with single primary antibodies selected to define cell identity and maturational stage, digitally scanned and compared to reveal the antigenic phenotype of individual cells.

Staining controls included positive and negative control tissues and primary antibody omission.

Imaging and analysis

Light microscopy

Light microscopy images up to ×100 objective magnification oil immersion were captured from a Zeiss Universal Research Microscope (Carl Zeiss Microscopy, Jena, Germany) fitted with a Leica DFC420 digital camera linked to Leica LAS version 3.8 software (Leica Microsystems, Wetzler, Germany).

Virtual microscopy

Slide-mounted sections were digitally scanned in an Aperio T2 ScanScope (Aperio Technologies, Vista, CA, USA). Using ImageScope software, the resultant virtual slide (.svs) image could then be analyzed at magnifications from slide overview up to ×40, with the software generating separate layers to permanently record cell counts and individual annotation details such as nuclear dimensions. Neuroglial cells were counted within standard area frames (0.2 mm^2) and more than five fields per marker averaged for expression as cells/mm^2 (± standard error of the mean; SEM) and as relative percentages of the total macroglia or neuroglia. With the .svs images of two or more differentially stained versions of the same or serial sections centered on the same cell and locked together, navigation around one image was matched on the others, allowing accurate comparison of staining outcomes. To ensure the correct staining designation of individual cells within virtual microscopy counting frames, sections were viewed concurrently by light microscopy at ×100.

Electron microscopy and electron microscopy—light microscopy correlation

Ultrastructural analysis of resin-embedded 80 nm sections mounted on slot aperture grids was carried out on a Jeol JEM-1400 digital transmission electron microscope (Jeol USA, Peabody, MA, USA). Low magnification electron microscopy digital image print outs were used as a link with individual cells in immunostained 1 μm sections, enabling direct correlation between ultrastructure and antigenic phenotype.

RESULTS

ECON model of antiserum-induced demyelination

Expression of HNK-1 by newly differentiated premyelinating oligodendrocytes correlates ultrastructurally with advanced axonal wrapping

One micron sections, cut serially to precede and follow "thin" (80 nm) electron microscopy (EM) sections, were immunostained as follows: glial fibrillary acidic protein (GFAP); vimentin (Vim); HNK; EM sections; HNK; myelin basic protein (MBP); griffonia simplicifolia isolectin II (GII). The resulting sections were then digitally scanned and compared as described in the Materials and Methods section to generate an antigenic phenotype for individual cells that could be correlated with their ultrastructural characteristics. In lesions timed at 9, 12, 17 and 24 days post lesion to precede and include remyelination, three maturational stages of oligodendrocyte lineage cells were identifiable: oligodendrocyte precursor cells (OPC; $GFAP^-/Vim^+/HNK^-/MBP^-/GII^-$); premyelinating oligodendrocytes (premyOl; $GFAP^-/Vim^-/HNK^+/MBP^-/GII^-$); and remyelinating oligodendrocytes (remyOl; $GFAP^-/Vim^-/HNK^+/MBP_{myelin}^+/GII^-$).

From the earliest time point (9 days post lesion), denuded axons were closely encircled by Vim intermediate filament-rich OPC processes. By 12 days post lesion, OPC differentiation into premyOls was occurring, with a switch from Vim to HNK expression in cell bodies and processes (Figure 1A,B). Ultrastructurally, intermediate filaments (Figure 1C) were replaced by microtubules set in cytoplasm with the inherent electron density characteristic of oligodendrocytes (Figure 1E). Investing processes exceeded one and a half wraps around individual axons (Figure 1F). By 17 days

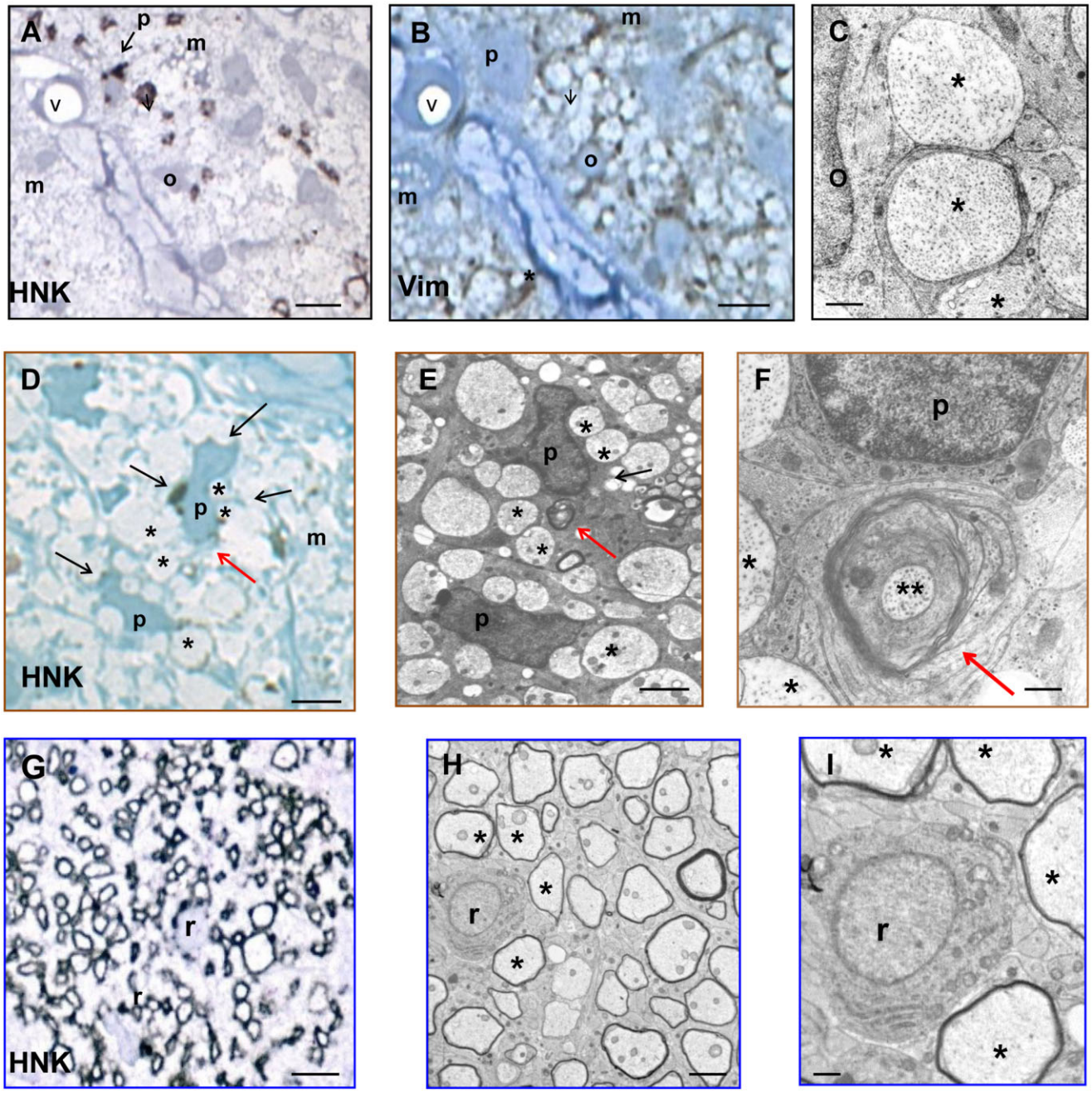

Figure 1. Immunohistochemistry, morphology and ultrastructure of oligodendrocyte lineage maturational stages in experimental remyelination. Experimental cat optic nerve (ECON) remyelination: Immunohistochemistry [A, D, G, HNK (human natural killer cell); B, Vim (vimentin)] and electron microscopy (C, E, F, H, I) of oligodendroglial differentiation stages involved in remyelination. A–F. 12 days post lesion. A, B. In serial 1 μm sections of a cross-sectioned fascicle bordered by connective tissue containing blood vessel "v," an oligodendrocyte precursor cell (OPC; o) and premyelinating oligodendrocyte (premyOl; p) show distinctive antigenic phenotypes; Vim^+ HNK^- (OPC); Vim^- HNK^+ (premyOl). D–F. An HNK^+ premyOl (p) is correlated with its ultrastructure in serial electron microscopy (EM) sections. Both precursor stages relate closely to the surrounding demyelinated axons (*), progressing from relatively simple process encirclement (OPC; C) to advanced wrapping (premyOl; F). Macrophage cytoplasm (m) is seen in A, B and D. G–I. 24 days post lesion. RemyOl (r) differentiation from premyOl is evidenced by the presence of compact myelin lamellae surrounding axons (H, I). Remyelinated axons are outlined by HNK^+ remyOl cytoplasm (G) but contiguity with the remyOl cell body can no longer be demonstrated. Scale bars = 10 μm (A, B, G); 5 μm (D, E, H); 1 μm (C, F, I).

Table 2. Human and experimental remyelination model tissue samples.
Abbreviations: C = experimental remyelination model cat optic nerve case; F = female; FF = formalin; M = male; MS = multiple sclerosis case; Mx = male neuter; n = number; NK = not known; PG = paraformaldehyde—glutaraldehyde; PMI = post-mortem interval.

Case code	Gender	Age (years)	PMI (hours)	Duration (years)	Tissue blocks (n)	Optic nerve segments (n)	Fixation
MS1	F	66	NK	8	3	7	FF
MS2	F	68	NK	NK	2	6	FF
MS3	M	63	NK	10	2	7	FF
MS4	M	40	NK	9	1	2	FF
				(days)			
C1	Mx	2	0	9	4	4	PG
C2	Mx	2	0	12	4	4	PG
C3	Mx	2	0	17	4	4	PG
C4	Mx	2	0	24	4	4	PG

post lesion, the proportion of OPC relative to premyOls had diminished and the appearance of thin compact myelin lamellae heralded the next maturational stage, that of remyOls. By 24 days post lesion, thin myelin sheaths surrounded most axons and all oligodendroglial cells were remyOls, sharing the same basic antigenic phenotype as premyOls (Vim^-/HNK^+) but with the additional expression of MBP in HNK^+ periaxonal processes that could no longer be demonstrated contiguous with cell bodies (Figure 1G–I). Common to all these lesion durations was the presence of debris-laden macrophages—throughout the parenchyma at earlier times (Figure 1A,B,D), with a generalized shift to perivenular locations as remyelination progressed.

MSON

When sections from the composite paraffin blocks containing segments of MSON (Table 2) were reacted with LFB counterstained with hematoxylin and eosin, myelin sheaths around axons were visible as bright blue-green rings or linear profiles depending on the plane of section, such that at low magnification, areas of demyelination appeared pale relative to adjacent myelinated tissue. Higher magnification revealed the thickness of myelin sheaths and whether cellularity in demyelinated areas was reduced or lacking heterogeneity. Also revealed was the quality of morphological preservation of individual segments and their orientation (transverse, oblique or longitudinal section). Particularly given the limitations inherent in formalin-fixed autopsy tissue, investigation was focused on segments displaying the highest quality of morphological and antigenic preservation, with further selection to those with cross-sectional physical orientation for the purposes of serial section analysis and accurate quantification.

Normal-appearing multiple sclerosis optic nerve (NAMSON)

Analysis of normal-appearing fully myelinated MSON provided a valuable comparison with the demyelinated lesions in addition to providing information on normality or otherwise relative to NHON. Seven NAMSON segments were identified from two cases (Table 3). Histologically, the main segment examined was fully myelinated, with no evidence of perivenular inflammation or neuroglial degeneration (case MS3; "N"; Figure 2A,G). The cross-sectional area fell within the normal range at approximately 9 mm^2 (30), and qualitatively, fiber density was not obviously diminished. Using cell-type-specific antigenic markers previously shown to reliably identify human neuroglia in formalin-fixed, paraffin-embedded sections (28) component cells were labeled and counted. Astrocytes were identified with antibody to GFAP or Vim (Figure 3D); microglia with Fcγ or CD68 (Figure 3C); oligodendrocytes with Olig1, Olig2, HNK, NoA, GS or CAII (Figure 3D–K); and NG2 cells/OP by Olig1 nuclear positivity (Figure 3F) or by Olig2 without cytoplasmic oligodendrocyte markers (Figure 3E). Oligodendrocytes, with nuclear diameters ranging from 6 to 10 μm, displayed the morphological

Table 3. Human and experimental optic nerve lesions and oligodendroglial cell types.
Abbreviations: — = no detailed analysis; C = experimental remyelination model cat optic nerve case; DM = demyelination; MS = multiple sclerosis case; N = normal-appearing MSON; "N" = example of N selected for detailed analysis; DMG = astrogliotic demyelination; "DMA" = demyelination lesion type A, selected for detailed analysis; "DMB" = demyelination lesion type B, selected for detailed analysis; OP = oligodendrocyte progenitor cell/NG2 cell; OPC = oligodendrocyte precursor cell; premyOl = premyelinating oligodendrocyte; R = remyelination; remyOl = remyelinating oligodendrocyte.

Case code	Predominant lesion type/s	*Oligodendroglial cell types in "specified lesions"
MS1	N/DMG/"DMB"	post remyOl†
MS2	N	—
MS3	N/DMG/"N"	OP/Ol
	"DMA"	OP/OPC/premyOl/remyOl
MS4	N/DMG	—
C1	R	OPC
C2	R	OPC/premyOl
C3	R	OPC/premyOl/remyOl
C4	R	remyOl

*Antigenic phenotype-based identification.
†post remyOl, best-fit classification based on combination of antigenic phenotype and nuclear dimensions (see the Results section).

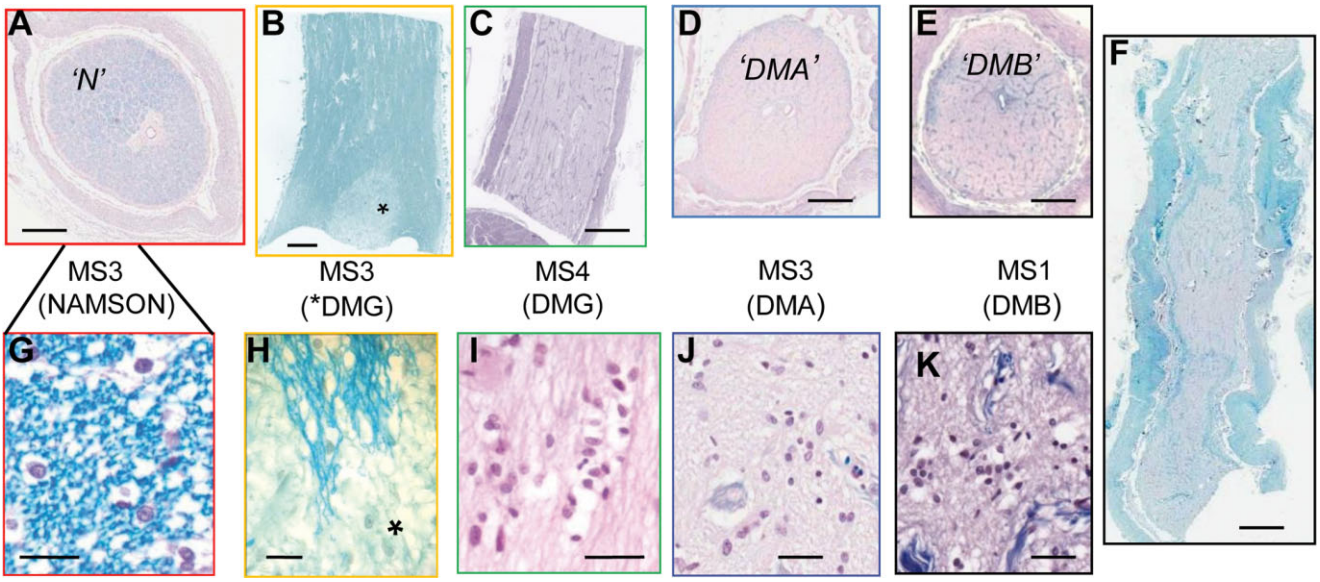

Figure 2. Normal-appearing and demyelinated optic nerve autopsy tissue segments from four cases of chronic multiple sclerosis (MS). Luxol fast blue (LFB) with hematoxylin and eosin counterstain. A–F. Low magnification overviews of transverse sections (A, D, E) and longitudinal sections (B, C, F). Myelinated areas were blue (A, B) compared with the relatively pale demyelinated lesions that in B and C–F occupied a small patch (*) or the entire nerve face, respectively. G–K. Higher magnification revealed myelin sheaths around axons as brightly stained rings (G) or linear profiles (H) as well as neuroglial cell abundance and basic nuclear morphology. (A, G; case MS3) Transected segment of normal-appearing multiple sclerosis optic nerve (**N**AMSON, "N"). At higher magnification (G), round oligodendrocyte nuclei among the myelinated axons are surrounded by a halo of cytoplasmic edema typical of post-mortem artifact. (B, H; case MS3) NAMSON containing a focal pale area (*) of astrogliotic demyelination [demyelination lesion type G (DMG)]. (C, I; case MS4) Totally demyelinated segment in longitudinal orientation. I. Higher magnification shows the typical DMG features of predominant uniform large astrocyte nuclei. (D, J; case MS3) Transected totally demyelinated segment [demyelination lesion type A (DMA)]. J. Higher magnification shows plentiful heterogeneous neuroglial cell nuclei. (E, K; case MS1) Transected totally demyelinated segment [demyelination lesion type B (DMB)]. K. Higher magnification shows plentiful heterogeneous neuroglial cell nuclei. (F; case MS1) Totally demyelinated segment in longitudinal orientation. Scale bars = 1 mm (A–F); 50 µm (G–K).

heterogeneity typically seen in NHON, often surrounded by a halo of edema that gave the typical "fried egg" appearance associated with post-mortem artifact (Figure 3B,G–J).

However, comparison of neuroglial counts with those in NHON revealed differences in both absolute and relative abundance. Although the total number of neuroglial cells per mm^2 was only slightly decreased, astrocytes were increased (260 cells/mm^2 vs. 205 cells/mm^2), whereas microglia (65 cells/mm^2 vs. 90 cells/mm^2), oligodendrocytes (290 cells/mm^2 vs. 340 cells/mm^2) and NG2 cells (18 cells/mm^2 vs. 35 cells/mm^2) were decreased. When expressed in terms of relative abundance, astrocytes comprised 41% (vs. 31%), microglia 10% (vs. 13%); oligodendrocytes 46% (vs. 51%) and NG2 cells 3% (vs. 5%). NG2 cells/OP were half as numerous as in NHON, with a ratio to oligodendrocytes of 1:16 (vs. 1:10).

Chronically demyelinated MSON lesions

In three of four cases, most segments displayed demyelination, with lesions occupying up to 100% of the nerve face (Figure 2C–E), including one extending longitudinally for more than 10 mm (Figure 2F). Astrogliotic demyelination (demyelination lesion type G; DMG) (Table 3), ranged from large, full-face plaques (Figure 2C) to relatively small patches located within NAMSON (Figure 2B,H) and typically featured reduced cellularity principally comprising cells with large, pale, ovoid nuclei (Figure 2I). In contrast, other demyelinated lesions contained plentiful, morphologically heterogeneous nuclei (Figure 2J,K), some of which labeled with the oligodendrocyte lineage marker, Olig2. To investigate the presence of oligodendroglia in these other chronic demyelination lesions, including their quantification relative to the other classes of neuroglia, detailed analysis was mainly focused on the best, representative, cross-sectioned segments; one each from cases MS1 and MS3. In both, the ON faces were totally demyelinated and markedly decreased in diameter relative to NHON and NAMSON (Table 4). Both lesions were quiescent, lacking dividing cells, perivenular cellular infiltrates, degenerate cells or debris-laden macrophages to indicate recent lesion activity. Hypertrophic astrocytes, some clustered together, with large, pale nuclei (up to 7 µm × 10 µm), were prominent.

However, clear differences were revealed by high magnification viewing of LFB staining and IHC to label oligodendrocytes (HNK). The two lesion types are hereafter referred to as demyelination lesion type A (DMA) (case MS3; Figure 2D,J) and demyelination lesion type B (DMB) (case MS1; Figure 2E,K). Whereas DMA featured an extensive matrix of inter- and

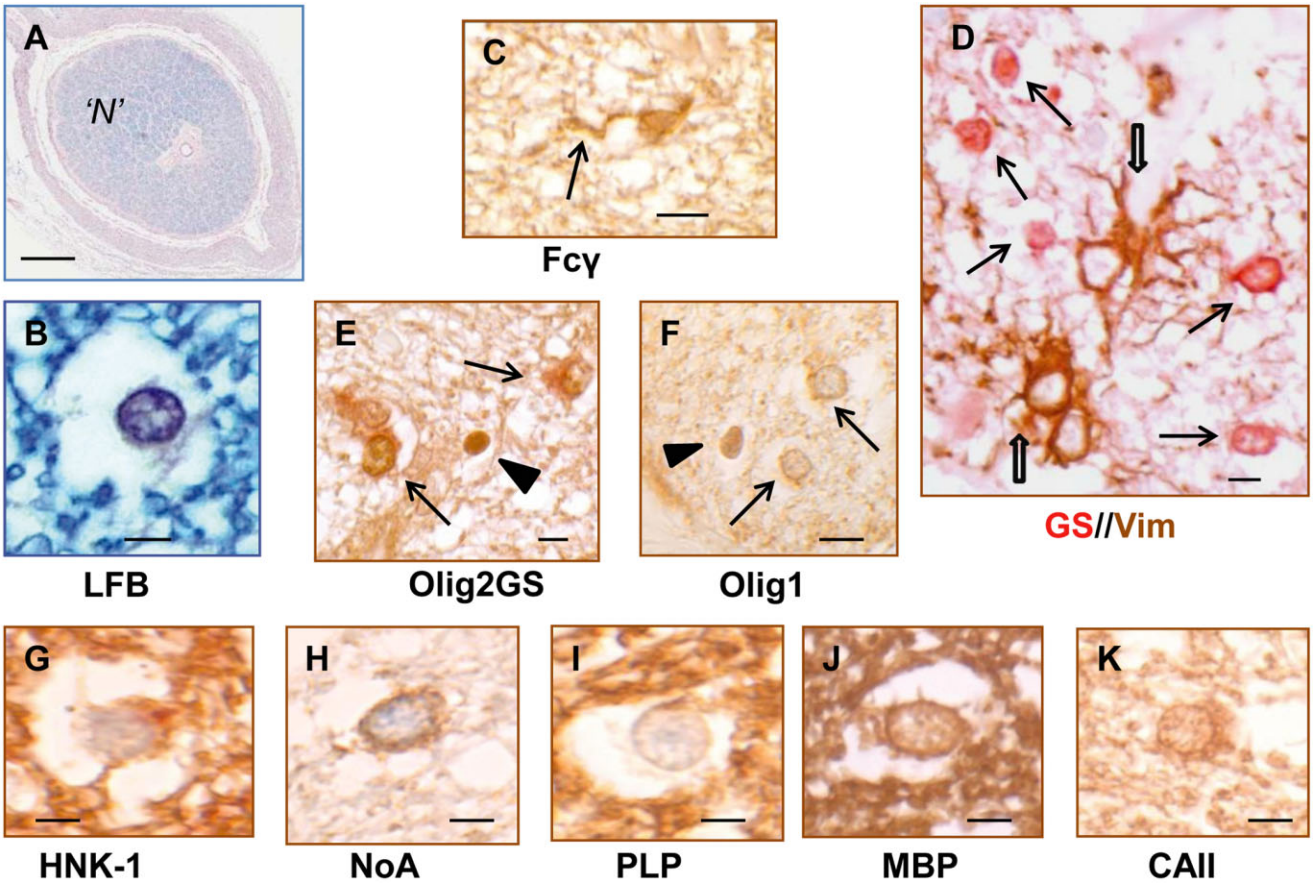

Figure 3. Morphology and immunohistochemistry of neuroglial cells in normal-appearing multiple sclerosis optic nerve (NAMSON). A, B. Luxol fast blue (LFB). NAMSON "N" was fully myelinated and exhibited high quality morphological preservation within the constraints of post-mortem autolysis and formalin fixation (eg, cytoplasmic edema in oligodendrocytes (B)]. D. Dual staining for vimentin (Vim; brown) and glutamine synthetase (GS; red): Vim$^+$ astrocytes (open arrows) often featured large nuclei and cell bodies with prominent coarse processes that extended among the smaller, round-bodied GS$^+$ oligodendrocytes (arrows). C. Fcγ$^+$ microglial cells were relatively inconspicuous and generally had small cell bodies extending into one or more long, spindly processes (arrow). E, F. NG2 cells/OP were distinguished either by relatively intense Olig2$^+$ (E, arrowhead) without oligodendrocyte cytoplasmic markers such as GS (arrows) or by nuclear Olig1 expression (F, arrowhead). D–K. Oligodendrocytes, in addition to nuclear Olig2, featured cytoplasmic labeling with GS (arrows in E), Olig1 (arrows in F), HNK (G), NoA (H) and CAII (K), with MBP (J) and PLP (I) generally restricted to myelin. Scale bars = 1 mm (A); 5 μm (B–K).

periaxonal oligodendroglial processes, with fine LFB$^+$ profiles in some fascicles, DMB not only lacked any myelin staining but had no evidence of axonal investment. To further compare the two lesion types, correlated morphological and IHC analysis was undertaken, with emphasis on the neuroglial complement and maturational stages of oligodendrocyte lineage cells. To this end, the SIMPLE protocol (24) was modified as described in the Materials and Methods section. Elements from a panel of antibodies (Table 1) were applied sequentially to individual sections, some of which had been pre-imaged with LFB, to allow unequivocal comparison of the staining pattern of two or more cell type- or oligodendroglial stage-specific markers, the relationship of oligodendroglial cells to axons stained for neurofilaments and/or evidence for cell division (Ki-67). Final counterstaining with solochrome cyanine revealed nuclear morphology and the presence of myelin sheaths.

DMA

Maturational stages of oligodendrocyte lineage cells in chronic demyelination relate to axons

In DMA, reduced numbers of transected nerve fibers were segregated into fascicles by variably thickened connective tissue septae (Figure 4A,B,E). Within all fascicles, hematoxylin staining revealed morphologically heterogeneous neuroglial cell nuclei. In addition to those typical of astrocytes, there were many darker, round to ovoid nuclei that were smaller than those of mature oligodendrocytes and featured aggregated heterochromatin and central nucleoli (Figure 4D–F). In sections stained with LFB and viewed at high magnification (×100 oil immersion), very thin LFB$^+$ profiles were visible in some fascicles as tight or loose periaxonal rings, depending on the extent of post-mortem artifact

Table 4. Neuroglial cell-type abundance in control and chronically demyelinated multiple sclerosis optic nerve.
Abbreviations: As = astrocytes; DMA = demyelination lesion type A; DMB = demyelination lesion type B; Mic = microglial cells; NAMSON = normal-appearing multiple sclerosis optic nerve; NHON = normal human optic nerve; Ol = oligodendrocytes/oligodendrocyte lineage cells; OP = NG2 cells/oligodendrocyte progenitor cells; Seg = segment; TS = transverse section.

Tissue/Seg (TS area)	Cells *	Total	As	Mic	Ol	OP
NHON†	Per mm^2	670	205	90	340	35
(~9 mm^2)	SEM	5.2	1.7	1.9	2.0	0.4
	%	100	31	13	51	5
NAMSON	Per mm^2	633	260	65	290	18
(9.5 mm^2)	SEM	6.9	3.8	0.7	1.9	0.3
	%	100	41	10	46	3
DMA	Per mm^2	600	260	65	225	5
(6.0 mm^2)	SEM	4.4	4.3	1.1	1.7	0.2
	%	100	43	11	38	<1
DMB	Per mm^2	650	335	145	170	0
(5.5 mm^2)	SEM	7.3	3.5	2.2	1.5	0
	%	100	52	22	26	0

*Counts averaged from multiple standard (0.2 mm^2) fields and expressed as cells per mm^2 and as a relative percent of the total neuroglia.
†Data from previous study (28).

(Figure 4E). The observation that these profiles also stained with solochrome cyanine histochemistry confirmed their identity as viable, albeit thin myelin sheaths are contiguous with oligodendroglial cell bodies. Fascicles containing such evidence of nascent remyelination were clustered together in two main foci (Figure 4A, outlined in red), separated from zones of total demyelination (Figure 4A, outlined in green) by fascicles exhibiting more scattered sheathing. The physical segregation of these patterns was maintained as sectioning progressed longitudinally (>2 mm).

Particularly in the fascicles with the most LFB staining, some oligodendroglial cell nuclei showed a clear spatial relationship to nearby myelinated axons, suggestive of them being remyOls (Figure 4D,H). However, the majority of the oligodendroglial cells, despite sharing similar nuclear morphology, were not associated with myelin sheathing (Figure 4F,G). Subsequent immunohistochemical analysis distinguished four oligodendroglial (Olig2$^+$) cell types on the basis of their antigenic phenotypes and staining expression patterns, none of which included cells undergoing division or apoptosis.

Almost all oligodendroglial cells expressed cytoplasmic Olig1 (weak; Figure 4Q), GS (Figure 4S), HNK (Figure 4I–L), NoA (Figure 4M,N) and PLP (Figure 4O,P). RemyOls (Figure 4D,H,L,N,P) were distinguished by perinuclear positivity visually separated from periaxonal (HNK, NoA) or myelin sheath staining (PLP, MBP). Some remyOl cytoplasm was weakly positive for MBP, p25 and CAII, which denotes oligodendroglial maturity (17, 26). In contrast, in the majority oligodendroglial cells not associated with myelin (Figure 5G,J,K,M,O), cell body positivity for HNK, NoA and PLP extended into radiating proximal processes, some of which contacted demyelinated axons, consistent with the morphology of PLP$^+$ cells described as premyOls in MS brain sections (14). Confirmation that the majority of axons were encircled by oligodendroglial cytoplasm was obtained by imaging for axonal neurofilaments followed by HNK (not shown). Occasional Vim$^+$ Olig2$^+$ cells with similar nuclei to the remyOls and premyOls (Figure 4R) had the Vim$^+$/HNK$^-$ antigenic phenotype typical of OPC in the ECON model (11), confirmed by imaging HNK staining followed by Olig2Vim. Rare NG2 cells/OP were demonstrated by nuclear expression of Olig1 (Figure 4Q) or by Olig2 in the absence of oligodendroglial cytoplasmic markers (Figure 4S) (28, 31, 34). Thus, component oligodendrocyte lineage cells were shown to comprise four separate entities identifiable by their antigenic phenotypes (Table 5) as (i) NG2 cells/OP (Olig1n$^+$/Olig2^{++}/Vim$^-$/HNK$^-$/NoA$^-$); (ii) OPC; Olig2$^+$/Vim$^+$/HNK$^-$/NoA$^-$); (iii) premyOl; (Olig2$^+$/Vim$^-$/HNK$^+$/NoA$^+$/PLP$^+$/CAII$^-$/MBP$^-$); and (iv) remyOl; (Olig2$^+$/Vim$^-$/HNK$^+$/NoA$^+$/PLP$^+$/p25$^+$/CAII$^+$/MBP$^+$).

Quantification (Table 4) revealed that the combined abundance of the oligodendroglial precursor stages was approximately two-thirds that of NHON oligodendrocytes (Ol) (225 cells/mm^2 vs. 340 cells/mm^2) and comprised 38% (vs. 51%) of the overall neuroglial complement. NG2 cells/OP were present in markedly reduced numbers (5 cells/mm^2 vs. 35 cells/mm^2), comprising <1% (vs. 5%) of neuroglia and with a ratio to the other oligodendroglial cells of 1:45 (1:10 Ol in NHON) (28). In contrast, astrocyte abundance was increased (260 cells/mm^2 vs. 205 cells/mm^2), comprising 43% of the total neuroglia. Qualitatively, wholly demyelinated fascicles contained a greater proportion of hypertrophic astrocytes that also tended to be clustered together. Heterogeneity among astrocytes was suggested by differential expression for the markers, GFAP and Vim, as well as between different Vim antibodies (Table 1). Microglia were not morphologically prominent, present in clusters or elevated in number (65 cells/mm^2 vs. 90 cells/mm^2), comprising 11% (vs. 13%) of the neuroglia. Only occasional perivenular microglial cells bore an activated antigenic phenotype (Fcγ^+/GII$^+$/Vim$^+$).

DMB

Oligodendroglial cells not associated with demyelinated axons

In DMB, the overall nerve atrophy relative to NHON was reflected internally where the fascicles were slightly shrunken despite the appearance of increased extracellular space (Figure 5A,B). With NF staining, nerve fibers were reduced in number, with considerable variation in both size and orientation of axonal profiles (Figure 5F). All fascicles contained plentiful, morphologically heterogeneous neuroglial nuclei (Figure 5C). Astrocytes positive for both GFAP and Vim were markedly increased relative to NHON (335 cells/mm^2 vs. 205 cells/mm^2; Table 4). Some were hypertrophic and clustered together and most featured long processes coursing among the axons (Figure 5D). Microglia were also elevated in number (145 cells/mm^2 vs. 90 cells/mm^2) and contributed extensive sinuous process profiles throughout the parenchyma (Figure 5E). Two morphologies were observed; the first were cells with small dark nuclei, limited cell body cytoplasm and fine, radiating processes that predominated over the second with larger cell bodies and relatively pale nuclei.

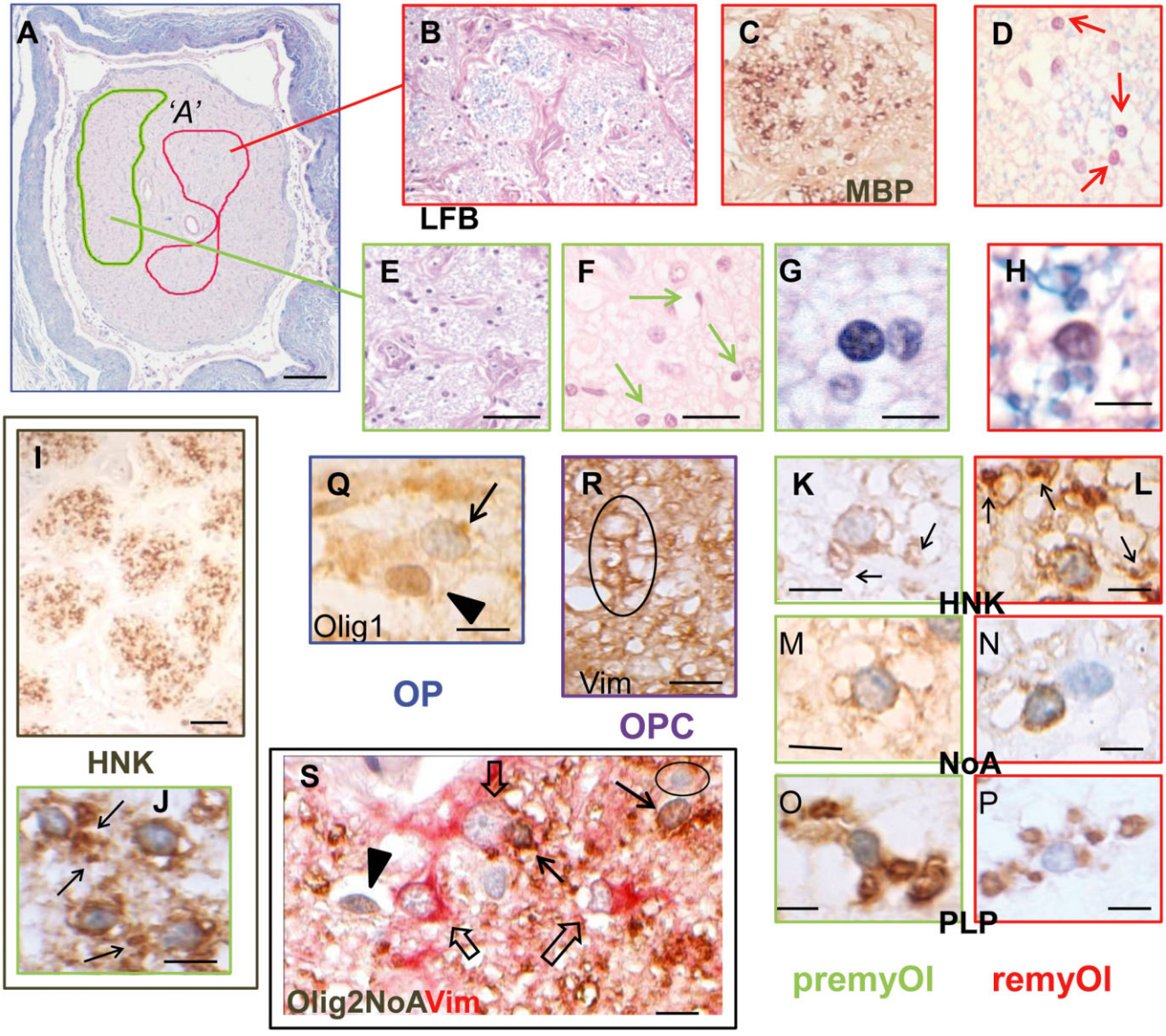

Figure 4. Morphology and immunohistochemistry of neuroglial cells in totally demyelinated multiple sclerosis optic nerve (MSON) with demyelination lesion type A (DMA). A, B, D–H. Luxol fast blue (LFB)-stained sections at overview (A) to high power magnification show the presence of cells with small round nuclei (arrows in D, F) that are closely associated with thin (MBP^+, C) myelin sheaths in some fascicles (outlined in red on overview, A and boxed in red; B–D, H) but not in others (outlined in green on overview, A and boxed in green; E–G). I–L. Immunohistochemistry with HNK labeled almost all of these cells, resulting in extensive staining throughout the demyelinated fascicles (I). J–L. At high magnification, HNK^+ staining was seen in two distinct patterns. J, K. In the majority premyOls (individual images boxed in green), radiating processes were seen extending out from perinuclear cell bodies to sometimes end in periaxonal cuffs (arrows), whereas remyOls (individual images boxed in red) lacked visible processes such that their perinuclear positivity was separated from nearby periaxonal rings (arrows in L). Further analysis showed a similar discriminative pattern with the markers NoA (M, N) and PLP (O, P). C. Immunohistochemistry with MBP was restricted to the thin myelin sheaths of remyOls. Q–R. In addition to premyOls and remyOls, antigenic phenotyping identified occasional OPC and OP. R. Following the SIMPLE (Sequential Immunoperoxidase Labeling and Erasing) protocol, an OPC nucleus at the top of the outlined example is faintly stained with haematoxylin remaining from the previous imaging stage and encircled by Vim+ cytoplasm that extends distally to wrap around nearby axons, (Vim preceding HNK and final counterstain). Q. NG2 cells/OP were identifiable by nuclear Olig1 expression (arrowhead) in contrast to premyOls or remyOls that had weak cytoplasmic staining (arrow). S. Dual staining identified multiple neuroglial cell types simultaneously within a single preparation. Olig2 combined with NoA (brown) and contrasted with Vim (red), separated premyOls or remyOls with small round (weakly) $Olig2^+$ nuclei and NoA^+ cytoplasm ($Olig2^+/NoA^+/Vim^-$; arrows) from NG2 cells/OP that had intense $Olig2^+$ nuclei but no cytoplasmic staining ($Olig2^+/NoA^-/Vim^-$; arrowhead), astrocytes with large nuclei and coarse straight processes ($Olig2^-/NoA^-/Vim^+$; open arrows) and immuno-negative microglia ($Olig2^-/NoA^-/Vim^-$; circled). Scale bars = 1 mm (A); 50 μm (E, I); 20 μm (F); 10 μm (P–R); 5 μm (G, H, J–S).

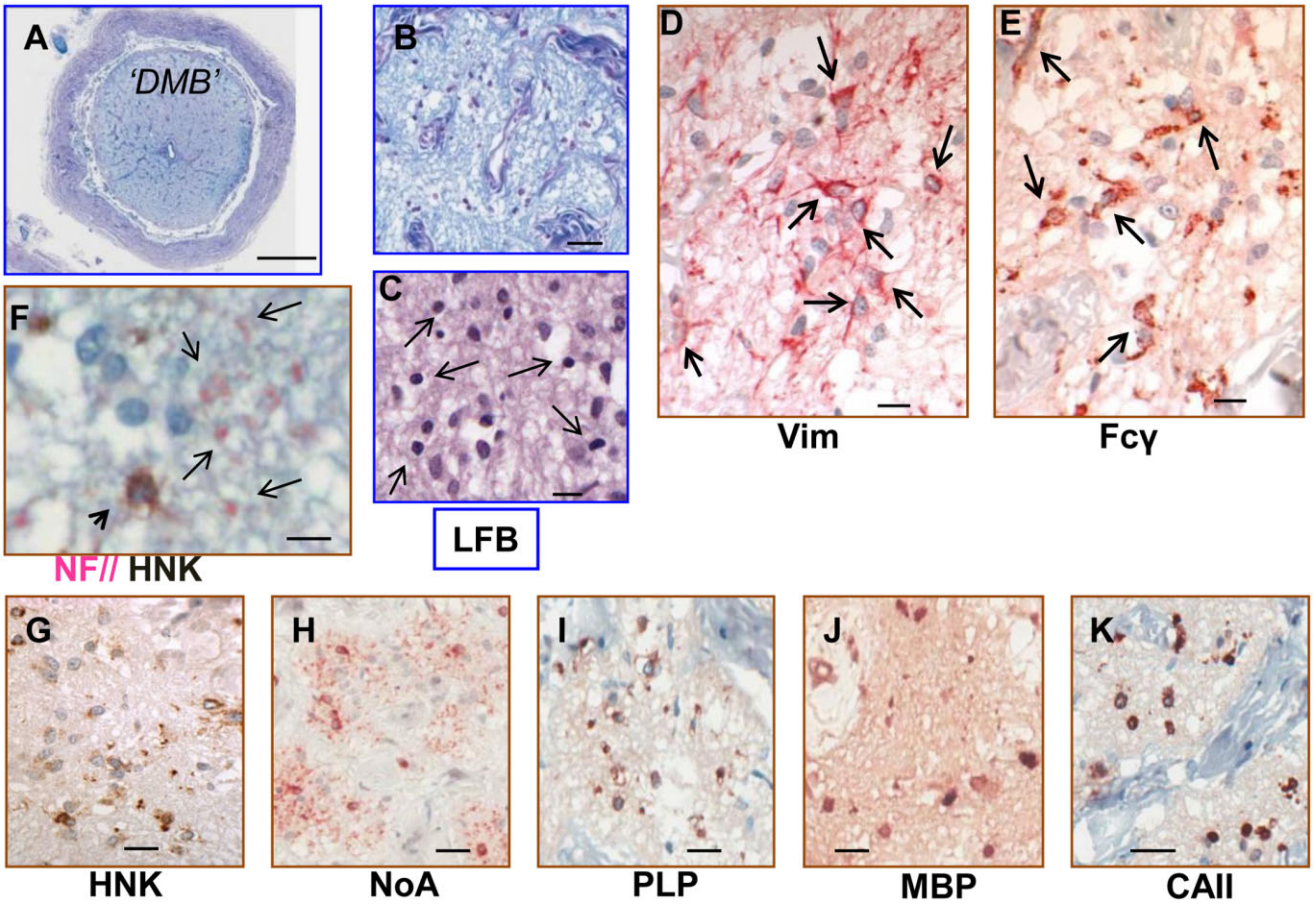

Figure 5. Morphology and immunohistochemistry of neuroglial cells in totally demyelinated multiple sclerosis optic nerve with demyelination lesion type B (DMB). A–C. Luxol fast blue (LFB)-stained sections at overview (A), low power (B) and high power magnification (C) show the presence within fascicles of numerous neuroglial cells with morphologically heterogeneous nuclei. D. Astrocytes were prominent (Vim; arrows). E. Staining with Fcγ (Table 1) revealed large numbers of morphologically heterogeneous microglia (arrows). C, F–K. Oligodendroglial cells with uniformly sized rounded (5–6 μm diameter) nuclei (arrows in C), all shared the mature antigenic phenotype HNK$^+$ (F, G)/NoA$^+$ (H)/PLP$^+$ (I)/MBP$^+$ (J)/CAII$^+$ (K) with positivity restricted to proximal cell body. F. The absence of axonal investment by processes from these cells was confirmed with dual staining to differentially label oligodendroglia (HNK; arrowhead; brown) and axonal neurofilaments (NF; examples arrowed; pink). Scale bars = 1 mm (A); 50 μm (B); 20 μm (G–K); 10 μm (C–F).

Olig2-positive oligodendroglial cells were present in all fascicles in reduced numbers relative to oligodendrocytes in NHON (170 cells/mm^2 vs. 340 cells/mm^2) and comprised only 26% of the total neuroglia (Figure 5C). Their round, 5 to 6 μm diameter nuclei (Figure 5C) were smaller than those of mature oligodendrocytes in NHON and NAMSON (Table 5). The impression of a uniform population was supported by the shared antigenic phenotype; Vim$^-$/HNK$^+$/GS$^+$/NoA$^+$/PLP$^+$/p25$^+$/MBP$^+$/CAII$^+$ (Table 5). In combination, nuclear size and the maturity level indicated by expression of myelin-associated proteins best fitted a differentiation status of "post remyOl" (advanced remyOl or immature oligodendrocyte). However, these cells did not appear normal. All cytoplasmic markers, including those known to reveal distal process extension (HNK; NoA), were largely restricted to proximal cell body cytoplasm (Figure 5F–K), with no evidence of axonal investment. Dual staining for NF and HNK confirmed that the occasional profiles of more distal oligodendroglial processes did not encircle demyelinated axons (Figure 5F). No NG2 cells/OP were identifiable.

DISCUSSION

Historically, knowledge about the pathology of MS has been built on the examination of tissue obtained at autopsy. While sections of MS lesions afford only a snapshot view of the pathological processes at the time of death, careful analysis can reveal much about the cells involved and likely events that have occurred. To the best of our knowledge, this study is the first to describe the IHC of chronic MS pathology in the normal-appearing and demyelinated human ON. We report the differential identification and abundance of the neuroglial complement based on our recent studies in the normal human ON (28).

Table 5. Antigenic phenotype of neuroglial cells in normal and demyelinated cat optic nerve; normal human optic nerve; normal-appearing multiple sclerosis optic nerve; chronically demyelinated multiple sclerosis optic nerve DMA* and DMB.
Abbreviations: As = astrocytes; $diam_n$ = approximate nuclear diameter; DMB = demyelination lesion type B; mic/ϕ = microglia/macrophage; my = myelin only; OI = mature oligodendrocytes; OP = NG2 cells/oligodendrocyte progenitor cells; OPC = oligodendrocyte precursor cells; premyOI = premyelinating oligodendrocytes; remyOI = remyelinating oligodendrocytes; v = variable/irregular; + = positive; ++ = intense positivity; – = negative; $+_n$ = nuclear positivity; $+_c$ = cytoplasmic positivity; $+_p$ = positivity extends into processes; –/* = negative except for activated microglia and macrophages.

Marker	Cell type	mic/ϕ	As	Oligodendrocyte lineage					
				OP	OPC	premyOI	remyOI	DMB	OI
$diam_n$ (μm)		v	8	v	4	5	5	5–6	6;7;8†
RCA		+	–	–	–	–	–	–	–
Fcg		+	–	–	–	–	–	–	–
GFAP		–	+	–	–	–	–	–	–
Vim		-/*	+	–	+	–	–	–	–
Olig1		–	–	$+_n$	$+_n$	$+_c$	$+_c$	$+_c$	$+_c$
Olig2		–	–	++	+	+	+	+	+
HNK		–	–	–	–	$+_p$	+	+	+
GS		–	–	–	–	+	+	+	+
NoA		–	–	–	–	$+_p$	+	+	+
PLP		–	–	–	–	$+_p$	+	+	my
MBP		–	–	–	–	–	+/-; my	+	+
GII		-/*	–	–	–	–	–	–	+
CAII		–	–	–	–	–	+/-	+	+

*Demyelination lesion type A oligodendroglial cells conformed to the antigenic phenotypes of OP; OPC; premyOI; remyOI.
†Mature oligodendrocyte subtypes OI1; OI2; OI3—data from previous study (28).

Interpretation of the findings was further aided by the ECON model of successful remyelination in which all oligodendroglial differentiation stages have been characterised (7, 11, 12). Given the antigenic concordance demonstrated between normal cat and human neuroglia (28), MS lesion cells could be referenced against the remyelinating oligodendrocyte lineage by their antigenic phenotype, thus predicting differentiation stage, ultrastructure and detailed relationship to the demyelinated axons. Of particular relevance, we confirm here that expression of HNK only appears once axonal investment by oligodendroglial precursor cell processes exceeds a complete wrap, as has been documented for Schwann cells during peripheral nervous system myelination (40).

The material examined and forming the basis of this report comprised four cases of MS (eight ONs) and is therefore neither claimed to be wholly representative of all MSON lesions, nor to fully capture the frequency with which the lesions described here might occur. Nevertheless, we believe that our findings add materially to the understanding of the histopathology of chronically demyelinated MSON. The observed differences in neuroglial quantification between NHON and the example of NAMSON (Table 4) despite its macroscopically normal appearance, serve to highlight the imperative for detailed direct analysis of MS tissue sections.

In addition to classic sclerotic plaques dominated by astrocytes (DMG), other totally demyelinated regions featured mixed neuroglial cell types including significant numbers of oligodendroglia. Although these lesions were all quiescent and stable, two main types (DMA and DMB) differed considerably, both in component oligodendrocyte lineage cells and in their relationship to demyelinated axons. DMA featured multiple oligodendrocyte precursor stages, the majority of which were engaged in axonal investment including some nascent remyelination, whereas DMB contained a uniform population of oligodendroglial cells that did not provide axonal investment. Together, these two lesion types provide important insights on the nature of chronically demyelinated MSON, which are especially relevant to the current understanding of remyelination failure.

DMA oligodendrocyte lineage cells totaled ~60% of the NHON complement (Table 4) and were shown to comprise rare NG2 cells/OP and OPC in addition to the predominant premyOl and remyOl. Although the presence of such axon-investing cells, some of which had elaborated thin myelin sheaths, could superficially suggest the commencement of early, successful remyelination, supporting evidence was lacking. There were no debris-laden macrophages as are typically found in both ECON and MS remyelination (3, 8). In MS, complete clearance of phagocytic cells indicates a longstanding lesion (3, 4). Nor was evidence found for a dynamic interplay between cell birth and death as was reported in a proportion of the original studies that identified oligodendrocyte precursor cells in chronic MS tissue sections (14, 18, 52). No evidence of ($Ki\text{-}67^+$) dividing cells was found and we do not consider that the many premyOls were short-lived as was concluded for morphologically similar, PLP^+ axon-associating "pre-myelinating oligodendrocytes" (14, 56). Rather, this lesion type appeared stable, implying that the axon-associating cells had been generated long ago and persisted long term. Although the past lesion environment evidently supported the majority of OPCs to differentiate into premyOls, relatively few had progressed to become remyOls, none of which had achieved full remyelination.

It is this scenario of remyelination failure despite the presence of potentially reparative cells that has become widely accepted as a common feature of chronically demyelinated MS lesions (32–34, 42). Numerous experimental studies have since generated hypotheses to explain why remyelination fails, stimulated by the prospect of promoting endogenous repair in MS (15, 22, 25, 35, 43–46, 50, 54, 64). A common assumption is that the cells involved are a homogeneous population of immature but otherwise normal, naive "OPC" (arbitrarily referred to as oligodendrocyte precursor or progenitor cells), prevented from progressing through to remyelination by external inhibitory factors (32–34). However, this view may be a serious oversimplification, with lack of contextual appreciation of the lesion environment underscoring the importance of direct MS lesion observation.

In the current study, several features suggested both heterogeneity of pathology and more complex dysfunction possibilities. Firstly, multiple oligodendrocyte precursor differentiation stages were present concurrently (OPC; premyOl; remyOl) including some progression to remyelination. Secondly, the majority premyOls with characteristic $HNK^+/NoA^+/PLP^+$ radial processes were unlikely to be normal *per se* as their longevity contrasted with the transient nature of this maturational stage in both successful remyelination (7) (ECON model, this study) and normal rodent development (56). Thirdly, possible axon-related dysfunction was suggested by the observation that the local limited remyelination foci were maintained longitudinally through serial sections, consistent with the extent of investment being specific to individual axons. It has been hypothesized that deficient, rudimentary myelination occurs when dysfunctional axons lack energy (ATP) to donate to the myelination process (50). Fourthly, NG2 cell/OP abundance was markedly reduced. In addition to their role as oligodendrocyte progenitors (OP) (28), NG2 cells have other important functions within the normal CNS, most of which involve intimate physical associations of their fine, far-reaching processes (16, 23, 28, 36, 47, 53, 63). Therefore, such pronounced NG2 cell loss, in addition to diminishing the ability to replace oligodendroglial cells, could have adversely affected the timely differentiation of the premyOls, particularly given the suggested role of NG2 cells in the establishment of nodes (5, 6, 21).

Further evidence of complexity was provided by the pathology evident in DMB despite superficial similarity to DMA of chronic demyelination in the presence of oligodendroglial cells. In contrast to the multiple axon-investing differentiation stages present in DMA, DMB oligodendroglial cells comprised a single, more differentiated population that lacked axonal associations and had an atypical proximal cell body staining pattern (Figure 5F–K) compared with mature oligodendrocytes (Figure 3D–K). In one of the earlier studies of chronically demyelinated MS brain, cells with a similar morphology and antigenic phenotype were described as "demyelinated oligodendrocytes," that is, mature oligodendrocytes that had survived the loss of their myelin sheaths (60). Our interpretation, particularly given the total absence of NG2 cells/OP and the smaller nuclear size of DMB cells relative to mature ON oligodendrocytes (Table 5), was that these cells had repaired a previous demyelination episode, reaching the differentiation stage of immature oligodendrocytes before axonal investment was subsequently lost. Potential reasons for this to occur include the scenario of so-called virtual hypoxia, whereby axoglial energy failure is proposed to lead to varying degrees of myelin and axonal loss (37, 55). Alternatively, other factors may have caused the lesion environment to become nonconducive for sustained axoglial relations. For instance, a switch of microglial activation can favor oligotoxic pro-inflammatory cytokines (38, 49). Certainly, microglial abundance in this lesion was markedly elevated in number and of mixed morphology. Environmental imbalance was also suggested by the increased numbers of astrocytes and the total absence of NG2 cells (Table 4).

Although remyelination has been shown to be the natural consequence of demyelination (8, 11, 48), many lesions in MS remain chronically demyelinated. Recent reports that some chronic lesions contain oligodendroglial cells are supported by our findings in the ON. However, the assumption that all such lesions display a uniform pathology of basically normal OPC that have failed to fully differentiate is not supported. Despite superficial similarities, oligodendroglia-containing chronic demyelination lesions are not necessarily the same, with implications for both hypotheses of remyelination failure and sampling for proteomics. Nevertheless, in terms of the goal to promote endogenous repair in MS, both lesion types described here revealed evidence suggestive of an initially successful response to large-scale demyelination, with extensive repopulation by OPC that had achieved advanced axonal investment. Particularly given the apparent stability of these lesions, it is therefore possible that a window of opportunity exists during which demyelinated axons are afforded physical protection and may retain electrophysiological function (10, 57) and whereby additional factors might be induced to act to afford longer term neuroprotection.

ACKNOWLEDGMENTS

We would like to thank Professor Margaret Esiri for facilitating provision of tissue blocks from the University of Oxford Willis Brain Bank, and Dr Wendy Macklin, Dr Ovadi and Professor Charles Stiles for the generous gift of antibodies. The study was supported by project grant funding from Multiple Sclerosis Research Australia (ARJ).

REFERENCES

1. Arnold AC (2005) Evolving management of optic neuritis and multiple sclerosis. *Am J Ophthalmol* **139**:1101–1108.
2. Audoin B, Fernando KTM, Swanton JK, Thompson AJ, Plant GT, Miller DH (2006) Selective magnetization transfer ratio decrease in the visual cortex following optic neuritis. *Brain* **129**:1031–1039.
3. Bruck W, Porada P, Poser S, Rieckmann P, Hanefeld F, Kretzschmar HA, Lassmann H (1995) Monocyte/macrophage differentiation in early multiple sclerosis lesions. *Ann Neurol* **38**:788–796.
4. Bruck W, Kuhlmann T, Stadelmann C (2003) Remyelination in multiple sclerosis. *J Neurol Sci* **206**:181–185.
5. Butt AM, Berry M (2000) Oligodendrocytes and the control of myelination *in vivo*: new insights from the rat anterior medullary velum. *J Neurosci Res* **59**:477–488.
6. Butt AM, Duncan A, Hornby MF, Kirvell SL, Hunter A, Levine JM, Berry M (1999) Cells expressing the NG2 antigen contact nodes of Ranvier in adult CNS white matter. *Glia* **26**:84–91.

7. Carroll WM, Jennings AR (1993) *In vivo* CNS remyelination: HNK-1 labels newly differentiated oligodendrocytes but not precursors. *J Neurocytol* **22**:583–589.
8. Carroll WM, Jennings AR (1994) Early recruitment of oligodendrocyte precursors in CNS demyelination. *Brain* **117**:563–578.
9. Carroll WM, Jennings AR, Mastaglia FL (1985) Galactocerebroside antiserum causes demyelination of cat optic nerve. *Brain Res* **330**:378–381.
10. Carroll WM, Jennings AR, Mastaglia FL, Levick WR (1985) Conduction in single nerve fibres in experimental demyelinative optic neuropathy. *Electroencephalogr Clin Neurophysiol* **61**:S178.
11. Carroll WM, Jennings AR, Mastaglia FL (1990) The origin of remyelinating oligodendrocytes in antiserum-mediated demyelinative optic neuropathy. *Brain* **113**:953–973.
12. Carroll WM, Jennings AR, Ironside LJ (1998) Identification of the adult resting progenitor cell by autoradiographic tracking of oligodendrocyte precursors in experimental CNS demyelination. *Brain* **121**:293–302.
13. Chan JW (2000) Optic neuritis in multiple sclerosis: an update. *Neurologist* **6**:205–213.
14. Chang A, Tourtellotte WW, Rudick R, Trapp BD (2002) Premyelinating oligodendrocytes in chronic lesions of multiple sclerosis. *New Engl J Med* **346**:165–173.
15. Chen CD, Sloane JA, Li H, Aytan N, Giannaris EL, Zeldich E *et al* (2013) The antiaging protein klotho enhances oligodendrocyte maturation and myelination of the CNS. *J Neurosci* **33**:1927–1939.
16. Dawson MRL, Polito A, Levine JM, Reynolds R (2003) NG2-expressing glial progenitor cells: an abundant and widespread population of cycling cells in the adult rat CNS. *Mol Cell Neurosci* **24**:476–488.
17. Diaz-Sanchez M, Williams K, DeLuca G, Esiri M (2006) Protein co-expression with axonal injury in multiple sclerosis plaques. *Acta Neuropathol* **111**:289–299.
18. Dowling P, Husar W, Menonna J, Donnenfeld H, Cook S, Sidhu M (1997) Cell death and birth in multiple sclerosis brain. *J Neurol Sci* **149**:1–11.
19. Ebers GC (1985) Optic neuritis and multiple sclerosis. *Arch Neurol* **42**:702–704.
20. Evangelou N, Konz D, Esiri MM, Smith S, Palace J, Matthews PM (2001) Size-selective neuronal changes in the anterior optic pathways suggest a differential susceptibility to injury in multiple sclerosis. *Brain* **124**:1813–1820.
21. Fancy SPJ, Baranzini SE, Zhao C, Yuk DI, Irvine KA, Kaing S *et al* (2009) Dysregulation of the Wnt pathway inhibits timely myelination and remyelination in the mammalian CNS. *Gene Dev* **23**:1571–1585.
22. Fancy SPJ, Harrington EP, Yuen TJ, Silbereis JC, Zhao C, Baranzini SE *et al* (2011) Axin2 as regulatory and therapeutic target in newborn brain injury and remyelination. *Nat Neurosci* **14**:1009–1016.
23. Frohlich N, Nagy B, Hovhannisyan A, Kukley M (2011) Fate of neuron-neuroglia synapses during proliferation and differentiation of NG2 cells. *J Anat* **219**:18–32.
24. Glass G, Papin JA, Mandell JW (2009) SIMPLE: a sequential immunoperoxidase labeling and erasing method. *J Histochem Cytochem* **57**:899–905.
25. Hagemeier K, Bruck W, Kuhlmann T (2012) Multiple sclerosis—remyelination failure as a cause of disease progression. *Histol Histopathol* **27**:277–287.
26. Harvey AR, Plant GW, Kent AP (1993) The distribution of astrocytes, oligodendroglia and myelin in normal and transplanted rat superior colliculus: an immunohistochemical study. *J Neural Transp Plas* **4**:1–14.
27. Jennings A, Carroll W (1999) GSLII positivity is not confined to oligodendrocytes in adult mammalian CNS. *J Neurocytol* **28**:239–248.
28. Jennings A, Carroll W (2010) Quantification of oligodendrocyte progenitor cells in human and cat optic nerve: implications for endogenous repair in multiple sclerosis. *Glia* **58**:1425–1436.
29. Jennings AR, Kirilak Y, Carroll WM (2002) *In situ* characterisation of oligodendrocyte progenitor cells in adult mammalian optic nerve. *J Neurocytol* **31**:27–39.
30. Jonas JB, Muller-Bergh JA, Schlotzer-Schrehardt UM, Naumann GO (1990) Histomorphometry of the human optic nerve. *Invest Ophth Vis Sci* **31**:736–744.
31. Kitada M, Rowitch DH (2006) Transcription factor co-expression patterns indicate heterogeneity of oligodendroglial subpopulations in adult spinal cord. *Glia* **54**:35–46.
32. Kotter MR, Stadelmann C, Hartung HP (2011) Enhancing remyelination in disease—can we wrap it up? *Brain* **134**:1882–1900.
33. Kremer D, Aktas O, Hartung HP, Kury P (2011) The complex world of oligodendroglial differentiation inhibitors. *Ann Neurol* **69**:602–618.
34. Kuhlmann T, Miron V, Cuo Q, Wegner C, Antel J, Bruck W (2008) Differentiation block of oligodendroglial progenitor cells as a cause for remyelination failure in chronic multiple sclerosis. *Brain* **131**:1749–1758.
35. Lau LW, Keough MB, Haylock-Jacobs S, Cua R, Doring A, Sloka S *et al* (2012) Chondroitin sulfate proteoglycans in demyelinated lesions impair remyelination. *Ann Neurol* **72**:419–432.
36. Lin SC, Bergles DE (2002) Physiological characteristics of NG2-expressing glial cells. *J Neurocytol* **31**:537–549.
37. Luessi F, Siffrin V, Zipp F (2012) Neurodegeneration in multiple sclerosis: novel treatment strategies. *Expert Rev Neurother* **12**:1061–1076.
38. Ma J, Tanaka KF, Shimizu T, Bernard CCA, Kakita A, Takahashi H *et al* (2011) Microglial cystatin F expression is a sensitive indicator for ongoing demyelination with concurrent remyelination. *J Neurosci Res* **89**:639–649.
39. Maeda Y, Solanky M, Menonna J, Chapin J, Li W, Dowling P (2001) Platelet-derived growth factor-[alpha] receptor-positive oligodendroglia are frequent in multiple sclerosis lesions. *Ann Neurol* **49**:776–785.
40. Martini R, Schachner M (1986) Immunoelectron microscopic localization of neural cell adhesion molecules (L1, N-CAM, and MAG) and their shared carbohydrate epitope and myelin basic protein in developing sciatic nerve. *J Cell Biol* **103**:2439–2448.
41. Moon LDF, Brecknell JE, Franklin RJM, Dunnett SB, Fawcett JW (2000) Robust regeneration of CNS axons through a track depleted of CNS glia. *Exp Neurol* **161**:49–66.
42. Nakahara J, Aiso S, Suzuki N (2009) Factors that retard remyelination in multiple sclerosis with a focus on TIP30: a novel therapeutic target. *Expert Opin Ther Targ* **13**:1375–1386.
43. Nakahara J, Kanekura K, Nawa M, Aiso S, Suzuki N (2009) Abnormal expression of TIP30 and arrested nucleocytoplasmic transport within oligodendrocyte precursor cells in multiple sclerosis. *J Clin Invest* **119**:169–181.
44. Patel JR, McCandless EE, Dorsey D, Klein RS (2010) CXCR4 promotes differentiation of oligodendrocyte progenitors and remyelination. *Proc Natl Acad Sci U S A* **107**:11062–11067.

45. Pedre X, Mastronardi F, Bruck W, Lopez-Rodas G, Kuhlmann T, Casaccia P (2011) Changed histone acetylation patterns in normal-appearing white matter and early multiple sclerosis lesions. *J Neurosci* **31**:3435–3445.
46. Piaton G, Aigrot MS, Williams A, Moyon S, Tepavcevic V, Moutkine I *et al* (2011) Class 3 semaphorins influence oligodendrocyte precursor recruitment and remyelination in adult central nervous system. *Brain* **134**:1156–1167.
47. Polito A, Reynolds R (2005) NG2-expressing cells as oligodendrocyte progenitors in the normal and demyelinated adult central nervous system. *J Anat* **207**:707–716.
48. Schmierer K, Parkes HG, So PW (2009) Direct visualization of remyelination in multiple sclerosis using T2-weighted high-field MRI. *Neurology* **72**:472.
49. Shimizu T, Tanaka KF, Takebayashi H, Higashi M, Wisesmith W, Ono K *et al* (2013) Olig2-lineage cells preferentially differentiate into oligodendrocytes but their processes degenerate at the chronic demyelinating stage of proteolipid protein-overexpressing mouse. *J Neurosci Res* **91**:178–186.
50. Sobottka B, Ziegler U, Kaech A, Becher B, Goebels N (2011) CNS live imaging reveals a new mechanism of myelination: the liquid croissant model. *Glia* **59**:1841–1849.
51. Soderstrom M, Ya-Ping J, Hillert J, Link H (1998) Optic neuritis: prognosis for multiple sclerosis from MRI, CSF, and HLA findings. *Neurology* **50**:708–714.
52. Solanky M, Maeda Y, Ming X, Husar W, Li W, Cook S, Dowling P (2001) Proliferating oligodendrocytes are present in both active and chronic inactive multiple sclerosis plaques. *J Neurosci Res* **65**:308–317.
53. Stallcup WB (2002) The NG2 proteoglycan: past insights and future prospects. *J Neurocytol* **31**:423–435.
54. Stoffels JMJ, de Jonge JC, Stancic M, Nomden A, Van Strien ME, Ma D *et al* (2013) Fibronectin aggregation in multiple sclerosis lesions impairs remyelination. *Brain* **136**:116–131.
55. Trapp BD, Stys PK (2009) Virtual hypoxia and chronic necrosis of demyelinated axons in multiple sclerosis. *Lancet Neurol* **8**:280–291.
56. Trapp BD, Nishiyama A, Cheng D, Macklin W (1997) Differentiation and death of premyelinating oligodendrocytes in developing rodent brain. *J Cell Biol* **137**:459–468.
57. Ulrich J, Groebke-Lorenz W (1983) The optic nerve in MS:a morphological study with retrospective clinicopathological correlation. *Neurol Ophthalmol* **3**:149–159.
58. Wolswijk G (1997) Oligodendrocyte precursor cells in chronic multiple sclerosis lesions. *Mult Scler* **3**:168–169.
59. Wolswijk G (1998) Chronic stage multiple sclerosis lesions contain a relatively quiescent population of oligodendrocyte precursor cells. *J Neurosci* **18**:601–609.
60. Wolswijk G (2000) Oligodendrocyte survival, loss and birth in lesions of chronic-stage multiple sclerosis. *Brain* **123**:105–115.
61. Wolswijk G (2002) Oligodendrocyte precursor cells in the demyelinated multiple sclerosis spinal cord. *Brain* **125**:338–349.
62. Xiao L, Guo D, Hu C, Shen W, Shan L, Li C *et al* (2012) Diosgenin promotes oligodendrocyte progenitor cell differentiation through estrogen receptor-mediated ERK1/2 activation to accelerate remyelination. *Glia* **60**:1037–1052.
63. Xu JP, Zhao J, Li S (2011) Roles of NG2 glial cells in diseases of the central nervous system. *Neurosci Bull* **27**:413–421.
64. Yuen TJ, Johnson KR, Miron VE, Zhao C, Quandt J, Harrisingh MC *et al* (2013) Identification of endothelin 2 as an inflammatory factor that promotes central nervous system remyelination. *Brain* **136**:1035–1047.